

Mixing in Simple Models for Turbulent Diffusion

ESTEBAN G. TABAK

AND

FABIO A. TAL

Courant Institute

Abstract

Simple turbulent diffusive models are proposed as conceptual tools for exploring scenarios involving mixing of stratified flows. Applications include the dynamics of the ocean's top mixed layer, shear instability, breaking internal waves, and turbulent stirring of sharp interfaces. A novel measure of mixing is developed, based on arguments from statistical physics. It is shown that, under turbulent diffusion, this measure grows, and that there are strong indications that, under stirring, flows tend to settle down at a maximum of this measure, subject to global dynamical constraints. © 2004 Wiley Periodicals, Inc.

1 Introduction

Mixing of water masses with different properties is ubiquitous in the ocean, and so is the mixing of air masses in the atmosphere. Identifying the forms and rates of mixing in both media is crucial to studying the climate and its variability. Yet how does a stratified flow mix?

There does not seem to be a single answer to this question. A great diversity of mixing scenarios exist, driven by quite different dynamical processes. When a dense fluid mass is placed above a lighter one, as when the ocean surface is cooled by cold winds, or when the bottom of the atmosphere is warmed by infrared radiation from the ground, a convective instability occurs, often resolved by vertically sinking (in the ocean) or rising (in the atmosphere) plumes or thermals. Nonuniform winds and currents generate shear instabilities, typically resulting in the shedding of mixing eddies. Pronounced internal waves may nonlinearly deform and overturn, leading to intense, localized mixing bursts.

Diverse as these scenarios are, they all share a common feature: flow instabilities give rise to highly turbulent bursts, which rapidly homogenize the local fluid properties. It is therefore attractive to treat them all under the common umbrella of turbulence-driven diffusion. Models of this kind are currently used in general circulation models [11]; in [2] they have been used to study the origin of the staircase density profiles of many oceanic settings (the latter article was one of the original sources of inspiration for the research described here). The idea behind the simplest of these models is to coarse-grain the dynamics of the small, unresolved

scales and locally replace the Navier-Stokes equations by a diffusive process. This diffusion is nonlinear, with a rate that depends on the local turbulent energy density (with turbulent energy defined as that contained in the unresolved scales).

In this article we look at a number of geophysically relevant mixing scenarios through the lens of simple turbulent diffusive models to illustrate the use of the latter as conceptual tools. We think of these as models of intermediate complexity, not as detailed as the full primitive fluid equations, but richer than the maximally reduced settings of most theoretical considerations. As such, they constitute an ideal test bench to validate theories, as well as an environment very well suited to developing intuition on complex fluid processes. In addition, these models are often simple enough that they can be subjected to rigorous mathematical analysis.

The topics visited in this article include the formation of well-mixed layers, the stability of sheared stratified flows, mixing by internal breaking waves, and an emerging theory of mixing that would predict the final state of a stirred fluid system by maximizing a suitable measure of disorder, subject to dynamical constraints. All these topics are the subject of active research; here they are given a relatively cursory view, intended to illustrate the versatility of simple turbulent diffusive models. Although such models can be used both for atmospheric and oceanic applications, we concentrate here on the latter, restricting attention to incompressible fluids.

It appears wise to end this introduction with a word of caution. The models described here are proposed as conceptual tools to aid in theory development and validation, and to build intuition on complex fluid phenomena (their use as subgrid parametrizations in general circulation models is already well established). Even though their output is often convincingly similar to real flows, these models do not follow directly from the primitive form of the fluid equations, but are built instead from heuristic and plausibility arguments. Their final form depends on tunable parameters and cannot therefore be considered as an accurate, first-principled representation of reality. The search for rigorous, formal, or even approximate closure schemes for turbulent diffusion is an area of active research and is not the topic of this article. (For a modern review, see [9] and references therein.)

2 A Mathematical Model for Turbulent Diffusion

In this section we describe a model for turbulent diffusion in some detail so that we can apply it in later sections to study a number of questions in fluid mixing. Models of this kind have been used extensively in ocean circulation models. The one that we present here enforces energy conservation, writing an evolution equation for the turbulent energy as in [2], and has no extra physical parametrizations, such as external forcing and energy dissipation into heat. We perceive it as one of the cleanest candidate models of intermediate complexity that facilitates the exploration of complex flows without resolving all the scales of the full fluid equations.

Since density variations in the ocean are very small, typically ranging below 3%, we shall adopt the Boussinesq approximation, whereby only the buoyancy effects of density variations are retained, while the variations of the fluid's inertia are neglected.

Our variables are the normalized density $b = g(\rho - \rho_0)/\rho_0$, where ρ is the fluid's density and ρ_0 a reference value (the letter b stands for buoyancy, though the fluid's actual buoyancy is $-b$); the normalized pressure P , which is the physical pressure divided by ρ_0 ; the velocity vector $\vec{u} = (u, v, w)$; and the turbulent kinetic energy per unit of mass e . We assume that both the buoyancy and the horizontal momentum are turbulently diffused, so that the equations of mass and horizontal momentum conservation are

$$(2.1) \quad b_t + \nabla \cdot (b\vec{u}) = \nabla \cdot (K_b \nabla b),$$

$$(2.2) \quad u_t + \nabla \cdot (u\vec{u}) - fv + P_x = \nabla \cdot (K_u \nabla u),$$

$$(2.3) \quad v_t + \nabla \cdot (v\vec{u}) + fu + P_y = \nabla \cdot (K_u \nabla v),$$

where f is the Coriolis parameter $2\Omega \sin(\alpha)$ (here Ω is the angular rate of rotation of the Earth and α is the latitude), and K_b and K_u are the turbulent diffusivities for buoyancy and shear, which we model below. The fbw is assumed incompressible, so we have

$$(2.4) \quad \nabla \cdot \vec{u} = 0.$$

In this article we shall make the extra assumption that the fbw is in hydrostatic balance:

$$(2.5) \quad P_z + b = 0.$$

This approximation is justified on the grounds that most geophysical applications have much larger horizontal than vertical extent. Clearly, at turbulent bursts, such as those produced by internal breaking waves or by convective plumes, the hydrostatic balance does not hold. Yet, in turbulent diffusive models, such turbulent bursts are not described in detail, but rather encompassed in the single quantity e and the accompanying enhanced diffusion. Therefore, there is no need to relax the hydrostatic approximation within these turbulent bursts.

Since we anticipate that the diffusivities K_b and K_u will depend on the local amount of turbulence present, characterized, for instance, by a typical value of the turbulent velocity field $U_T \sim \sqrt{e}$, still another equation is needed in order to close the system. Our choice is an equation for the diffusion of the turbulent energy itself, which reads

$$(2.6) \quad e_t + \nabla \cdot (e\vec{u}) = \nabla \cdot (K_e \nabla e) + K_b b_z + K_u (|\nabla u|^2 + |\nabla v|^2).$$

The first term on the right-hand side represents diffusion of turbulent energy, with diffusivity K_e , while the others are required for the total energy

$$\int \left(zb + \frac{|\vec{u}_h|^2}{2} + e \right) dV$$

to be preserved by the fbw. (Here $\vec{u}_h = (u, v)$ represents the horizontal components of the velocity vector.) The physical interpretation of these extra terms is straightforward. The first, a sink, represents the energetic cost of mixing a stratified fluid, raising heavy and bringing down light parcels of fluid. The second, a source, accounts for the energy surplus provided by homogenizing momentum, stemming from the mathematical fact that the square of the average velocity is smaller than the average of the velocity squared. The conservation law associated with (2.6) is that of the total energy; it reads

$$(2.7) \quad \left(zb + \frac{|\vec{u}_h|^2}{2} + e \right)_t + \nabla \cdot \left(\left(zb + \frac{|\vec{u}_h|^2}{2} + e + P \right) \vec{u} \right) = \nabla \cdot \left(K_e \nabla e + K_b z \nabla b + K_u \nabla \frac{|\vec{u}_h|^2}{2} \right).$$

Finally, we must determine the turbulent diffusivities. One reasonable assumption is that each diffusivity must be proportional to the mean turbulent velocity. In order to simplify our approach, we will assume this simplest scenario and set

$$(2.8) \quad K_j = l e^{\frac{1}{2}} S_j \quad \text{for } j \in \{b, u, e\},$$

where l is some fixed-length scale, “the typical size of a mixing eddy,” and the S_j ’s are dimensionless parameters accounting for the possibly different mixing rates for the various physical quantities of the system.

Other models may be produced by treating l not as a constant but as a function of the dependent variables. Dimensional analysis suggests the possibilities

$$l = \sqrt{\frac{e}{b_z}}, \quad l = \sqrt{\frac{u^2}{b_z}}, \quad \text{and} \quad l = \sqrt{\frac{e}{(u_z)^2}}.$$

Still another possibility is to let l evolve dynamically, modeling the cascade of turbulent energy across scales. In this note, however, we concentrate on the simple choice that has l fixed at some externally provided value. The arbitrariness of this value should work as a reminder that treating turbulent mixing as a diffusive process is not a first-principled approach, but a convenient, often deceptively convincing closure. Implementations of turbulent diffusive parametrizations in general circulation models tune this parameter to match real-world observations.

3 Quantifying Mixing

Fluid mixing, a key process in climate studies, is also quite elusive. How can one define the effectiveness of mixing by various physical processes, and how can one measure mixing in a physical laboratory experiment, in the real ocean and atmosphere, and in output from numerical simulations? The latter is particularly relevant to us here. In this section, we develop the rudiments of a theory for measuring the degree of mixing of a fbw. As we shall see in Section 4.1 (see also [6]), the proposed measure may well not only serve for quantifying the output of

simulations, but also yield as a bonus an accurate dynamical closure for mixing processes. A definition of the mixing rate of stratified fluids often used in physical oceanography (see, for instance, [13] and references therein) builds on the concept of available potential energy [8]; we follow here a radically different approach, where we distinguish the quantification of the mixing process itself from the various dynamical constraints to which it is subject, such as energy conservation. This approach, based on statistical considerations, bears a strong resemblance to the description of turbulent vortical fields through large-deviation principles, as described, for instance, in [3] and references therein.

In order to quantify mixing, we will follow the conceptual framework of statistical physics, computing the number of microstates consistent with a given macrostate. We concentrate here on the mixing of two fluids α and β , with corresponding densities ρ_α and ρ_β , where $\rho_\beta > \rho_\alpha$. To bypass the subtleties associated with the statistical description of continuous media, we adopt a discrete approach, whereby we regard space as a fixed lattice, with a fluid particle of type either α or β in each node. To talk about macrostates, one needs to coarse-grain the system. We shall therefore partition the lattice into patches with n_j nodes each, with $1 \ll n_j \ll N$, where N represents the number of lattice points in the area of interest. The density in patch j is given by

$$(3.1) \quad \rho = \frac{m_j}{n_j} \rho_\beta + \frac{n_j - m_j}{n_j} \rho_\alpha$$

where m_j is the number of β particles in the j^{th} patch. It is convenient to introduce the normalized density ρ^* :

$$(3.2) \quad \rho^* = \frac{\rho - \rho_\alpha}{\rho_\beta - \rho_\alpha} = \frac{m_j}{n_j}.$$

The number of particle distributions consistent with a given macrostate is given by

$$(3.3) \quad N_d = \prod_j \binom{n_j}{m_j} = \prod_j \frac{n_j!}{m_j! (n_j - m_j)!}.$$

For our measure S of mixing to be additive, we shall adopt the logarithm of N_d (normalized by $\frac{N}{V}$, the number of lattice points per unit volume), and invoke the fact that n_j , m_j , and $(n_j - m_j)$ are large numbers to use Stirling's approximate formula for the logarithm of the factorials:

$$(3.4) \quad \begin{aligned} S &= \frac{V}{N} \log(N_d) \\ &= \frac{V}{N} \sum_j \log(n_j!) - \log(m_j!) - \log((n_j - m_j)!) \\ &\approx \frac{V}{N} \sum_j n_j \log(n_j) - m_j \log(m_j) - (n_j - m_j) \log(n_j - m_j) \end{aligned}$$

$$\begin{aligned}
&= -\frac{V}{N} \sum_j n_j \left(\frac{m_j}{n_j} \log \frac{m_j}{n_j} + \frac{n_j - m_j}{n_j} \log \frac{n_j - m_j}{n_j} \right) \\
&= -\sum_j V_j (\rho^* \log(\rho^*) + (1 - \rho^*) \log(1 - \rho^*)),
\end{aligned}$$

where

$$V_j = \frac{n_j}{N} V$$

is the volume of patch j . As the lattice grows denser, clearly (3.4) converges to

$$(3.5) \quad S \stackrel{\text{def}}{=} - \int_V (\rho^* \log(\rho^*) + (1 - \rho^*) \log(1 - \rho^*)) dV,$$

which, together with (3.2), constitutes our sought quantification of the degree of mixing of a particular density distribution when it arises from stirring together two homogeneous fluid masses. This measure is entirely analogous to the classical statistical mechanical measure of mixing ideal gases [7].

Notice that S can only increase with time if there are no fluxes of buoyancy through the boundaries, in agreement with the irreversibility of mixing processes. This follows from the following calculation:

$$\begin{aligned}
(3.6) \quad \frac{dS}{dt} &= \int_V \frac{\delta S}{\delta \rho^*} \frac{d\rho^*}{db} \frac{db}{dt} \\
&\quad - \int_V (\log(\rho^*) - \log(1 - \rho^*)) \lambda \nabla \cdot (K_b \nabla b) dV \\
&= \int_V \lambda^2 \left(\frac{1}{\rho^*} + \frac{1}{1 - \rho^*} \right) K_b (\nabla b)^2 dV
\end{aligned}$$

where $\lambda = d\rho^*/db > 0$ is a constant. Hence S is always strictly increasing except when b is a constant or when K_b is zero everywhere, so no mixing can occur.

4 One-Dimensional Applications

When we assume horizontal homogeneity, the system of equations (2.1) through (2.6) assumes the simpler form

$$\begin{aligned}
b_t &= (K_b b_z)_z, \quad u_t - fv = (K_u u_z)_z, \quad v_t + fu = (K_u v_z)_z, \\
e_t &= (K_e e_z)_z + K_b b_z + K_u (u_z^2 + v_z^2).
\end{aligned}$$

If, in addition, we neglect the effects of the earth's rotation, and consider only fbws in the plane (x, z) , the system above simplifies further to

$$(4.1) \quad b_t = (K_b b_z)_z,$$

$$(4.2) \quad u_t = (K_u u_z)_z,$$

$$(4.3) \quad e_t = (K_e e_z)_z + K_b b_z + K_u u_z^2.$$

In this section we apply this one-dimensional model to study the diapycnal mixing of two fluid layers driven by an injection of turbulent energy at their interface, the dynamics of the ocean's well-mixed layer, and the shear stability of stratified flows.

To solve the equations numerically, we use finite differencing in conservation form. The conserved quantities b , u , and e are represented by their averages over numerical cells, while the fluxes are computed by interpolation at the interfaces between cells. These fluxes are further limited so as to proscribe negative turbulent energies: at every time step, the buoyancy is only allowed to diffuse up to the available turbulent energy. Second-order accuracy in time is achieved through a predictor-corrector scheme.

4.1 Turbulent Mixing of a Sharp Interface

Consider a density profile consisting of two semi-infinite homogeneous layers of densities ρ_a and ρ_b , the lighter one above, separated by a sharp interface at $z = 0$. Without an external supply of energy, the two layers cannot mix, since diapycnal mixing is energetically costly. Suppose, though, that an amount E of turbulent energy is injected into the flow at time zero, concentrated at or near the interface. (Such energy injections in real flows arise due to shear instabilities and to breaking waves. Another turbulent energy source, the thermobaric effect, has recently been advanced as a novel candidate mechanism for polynya formation in Antarctica.) Then the flow will mix locally until all the turbulent energy is consumed, and the question arises as to what the final density profile will look like. Clearly this final profile is constrained by conservation of mass and energy; however, these two constraints fall short of providing enough information to determine the full functional dependence of the density ρ on the depth z .

A tempting approach here is to propose a scenario reminiscent of statistical physics: of all the profiles compatible with the available dynamical constraints (i.e., conservation of mass and energy), choose the one that maximizes the amount of mixing, as encompassed in definition (3.5). In this subsection, we perform such maximization and compare the resulting profile with the one arising from the numerical simulation of the model in (4.1)–(4.3).

If we adopt units such that the normalized density b is 0 in the upper layer and 1 in the lower, then b can be identified with ρ^* in (3.2), so S (from (3.5)), the function to maximize, becomes

$$(4.4) \quad S = \int_{-\infty}^{\infty} (b \log(b) + (1 - b) \log(1 - b)) dz,$$

subject to the constraints that

$$(4.5) \quad \int_{-\infty}^{\infty} (b - b_0) dz = 0 \quad (\text{conservation of mass})$$

and

$$(4.6) \quad \int_{-\infty}^{\infty} (b - b_0)z \, dz = E \quad (\text{conservation of energy})$$

where

$$b_0 = \begin{cases} 0 & \text{for } z > 0 \\ 1 & \text{for } z < 0. \end{cases}$$

It is convenient to symmetrize the problem, shifting the origin for the density:

$$\rho = b - \frac{1}{2}.$$

In terms of ρ and the two Lagrange multipliers μ and λ for the mass and energy constraints, respectively, one needs to look for stationary profiles over all functions $\rho(z)$ for the following functional:

$$F = \int_{-\infty}^{\infty} \left(\left(\frac{1}{2} + \rho \right) \log \left(\frac{1}{2} + \rho \right) + \left(\frac{1}{2} - \rho \right) \log \left(\frac{1}{2} - \rho \right) + \left(\rho + \frac{s}{2} \right) (\mu + \lambda z) \right) dz$$

where $s = \text{sign}(z)$. The variational derivative with respect to ρ yields

$$(4.7) \quad \log \left(\frac{\frac{1}{2} + \rho}{\frac{1}{2} - \rho} \right) + \mu + \lambda z = 0.$$

In order to satisfy (4.5) and (4.6), we need to set $\mu = 0$ (i.e., $\rho(z)$ is an odd function) and $\lambda = -\pi/\sqrt{6E}$, so $\rho(z)$ is given by

$$(4.8) \quad \rho = \frac{1}{2} \frac{e^{-\pi z/\sqrt{6E}} - 1}{e^{-\pi z/\sqrt{6E}} + 1}.$$

In Figure 4.1 we plot $\rho(z)$ both from (4.8) and from a numerical simulation of equations (4.1) and (4.3) with $E = 7$. We have solved the problem in a finite domain, with z ranging from -50 to 50 . Clearly, the boundaries are far enough that they exert no influence over the numerical solution. The agreement of the two curves is remarkable, both for buoyancy values and for the size of the transitional layer.

4.2 The Ocean's Well-Mixed Layer

Throughout the world's ocean, there exists a well-mixed top layer, with a typical vertical extent ranging from 50 to 100 meters. In this layer, stirring causes the density to be almost independent of depth, unlike the ocean's deeper interior, which is stably stratified. The bottom of the well-mixed layer often develops high-density gradients, becoming the most prominent feature of the pycnocline. Capturing the dynamics of the mixed layer accurately is a challenging, yet critical task for general circulation models, since it is through this layer that all heat and momentum exchanges between the ocean and the atmosphere take place. Recent laboratory work

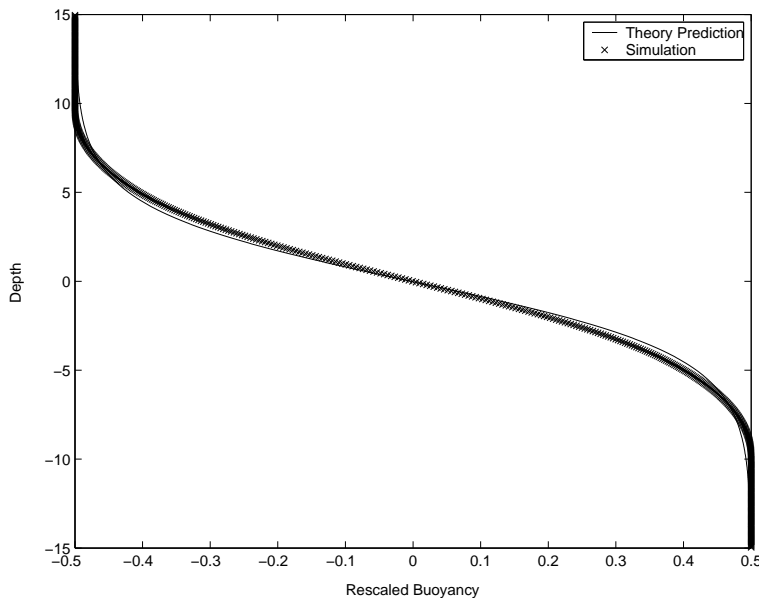


FIGURE 4.1. Buoyancy profile resulting from the mixing of two initially distinct layers, subject to an injection of turbulent energy at their interface. The two profiles displayed correspond to the theoretical prediction based on maximal mixing and to the actual numerical results following the dynamics of the turbulent diffusive model.

on fluid entrainment into well-mixed layers can be found in [14] and references therein.

The origin and dynamics of the mixed layer depends on latitude, season, and situation. Mechanical stirring occurs when storms generate turbulence through wave breaking and shear instability at the ocean's surface. The turbulent energy is then nonlinearly diffused through the layer and generates mixing at its bottom, thus entraining water from the ocean's interior and increasing the layer's depth. Buoyancy-driven stirring takes place when the ocean's surface experiences buoyancy losses, due either to cooling or to salinity increments due to evaporation and freezing. When the surface layers of the ocean become heavier than the interior, convection occurs. This in turn releases potential energy that is transformed into turbulence, inducing further mixing.

To illustrate the well-mixed layer dynamics generated by the turbulent model (4.1), (4.2), and (4.3), we perform two numerical experiments in which the atmospheric influence is represented by boundary fluxes. For conciseness, we combine in the first experiment boundary fluxes of buoyancy and turbulent energy (see [15] for a separate account of the two mechanisms), while in the second one we treat the case of momentum flux. In our experiments, the eddy mixing length l is set to $\frac{1}{4}$, and the diffusivities S_b , S_u , and S_e are set to 1. The initial vertical profile for the

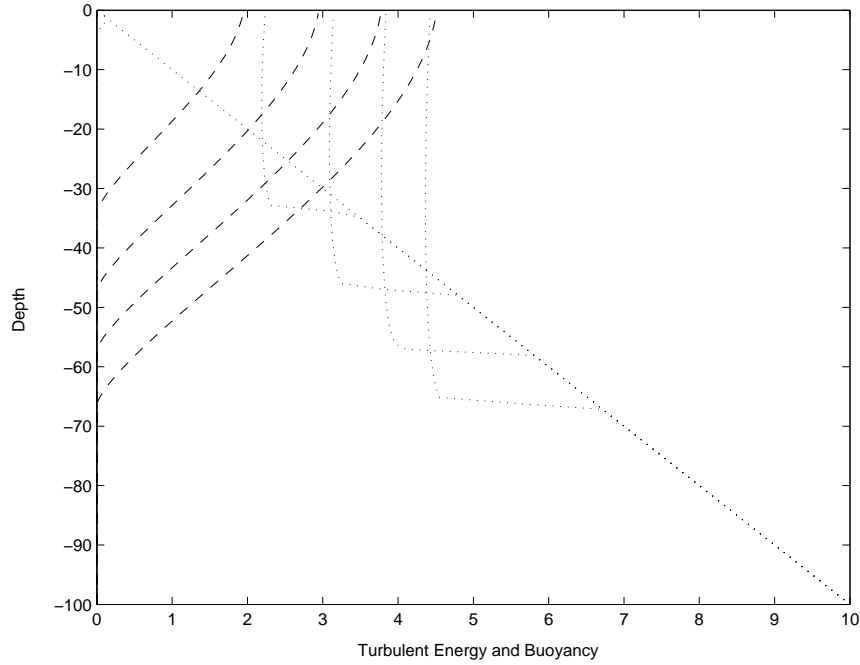


FIGURE 4.2. Formation of a well-mixed layer in a stratified fluid by a constant flux of buoyancy and turbulent energy from the top. The dotted line represents the buoyancy profile, and the dashed line the turbulent energy. The snapshots plotted are 9000 time units apart. The energy flux through the top surface is given by $K_e e_z = 0.005$, and the buoyancy flux by $K_b b_z = 0.002$.

buoyancy is linear, representing a background stratification, and the velocity profile is initially depth independent. Finally, the turbulent energy is initialized as 0 everywhere except for some small initial turbulence close to the surface, necessary in our model to start the boundary fluxes. In the first experiment, the boundary fluxes at the ocean's surface are constant: 0 for horizontal momentum, 0.002 for buoyancy, and 0.005 for turbulent energy.

The numerical solution at times 9000 units apart is displayed in Figure 4.2. A remarkable feature is the large gradients appearing at the bottom of the mixed layer, which becomes in fact discontinuous. Our model is diffusive, and diffusion is usually associated with attenuation of disparities, but in this case the strongly nonlinear nature of this diffusion yields the inverse phenomenon. This counterintuitive and mathematically appealing feature is in good agreement with physical reality.

Another interesting feature is that the rate of growth of the mixed layer slows down considerably as the storm progresses. This can be understood by a simple energetic argument, where the mixed layer is taken to be completely homogeneous,

with the same buoyancy throughout its depth. If $b = -g'z$ is the linear background stratification of the ocean, and the mixed-layer thickness is H , mass conservation implies that the density in the layer is $\bar{b} = (g'H)/2$. Then, if the mixed layer is deepened to $H + \Delta H$, the potential energy increase is

$$\begin{aligned} \Delta \text{PE} &= \int_{-H}^0 \left(\frac{g'(H + \Delta H)}{2} - \frac{g'H}{2} \right) z \, dz \\ &\quad + \int_{-H-\Delta H}^{-H} \left(\frac{g'(H + \Delta H)}{2} + g'z \right) z \, dz \\ &= g' \frac{\Delta H H^2}{4} + O((\Delta H)^2). \end{aligned}$$

So we see that the work per unit time required for the growth of the mixed layer increases as the square of the depth, explaining the reduced velocity observed in the numerical runs.

In the second experiment (Figure 4.3), a boundary flux of momentum accounts for the action of the wind. We see a substantial horizontal velocity developing near the surface and diffusing rapidly, due to the turbulence generated by shear instability throughout the mixed layer. Hence the mixed layer decouples from the bulk of the ocean, developing a mean velocity of its own. The base of the mixed layer is smoother here than in the previous experiment, since turbulence is more effectively generated precisely at this interface, which has the maximum shear. Hence diffusion is locally enhanced, and the potential discontinuity at the base is smoothed away.

4.3 Shear Instability and the Richardson Number

An inhomogeneous velocity field constitutes a reservoir of energy: if a flow were to be locally uniformized while preserving its total momentum, there would remain a surplus of kinetic energy. Hence shear is a source of instability. However, for stratified, vertically sheared flows, local mixing uniformizes not just the momentum but also the density. The latter process *consumes* energy, since it involves raising heavy fluid parcels and lowering lighter ones. Hence the relevance of the Richardson number

$$\text{Ri} = -\frac{b_z}{(u_z)^2},$$

which measures the relative strength of the stabilizing influence of the stratification versus the destabilizing influence of the shear. In classical work [5, 12], the significance of the Richardson number was established, as well as an upper bound of $\text{Ri} = \frac{1}{4}$ for a steady, horizontally uniform flow to be linearly unstable within the framework of the incompressible Euler equations of motion.

In this section we analyze the shear instability of horizontally homogeneous, stratified flows within the simplified dynamics of the model in (4.1), (4.2), and (4.3). We start with a qualitative stability analysis, illustrated by numerical simulations and followed by some rigorous results.

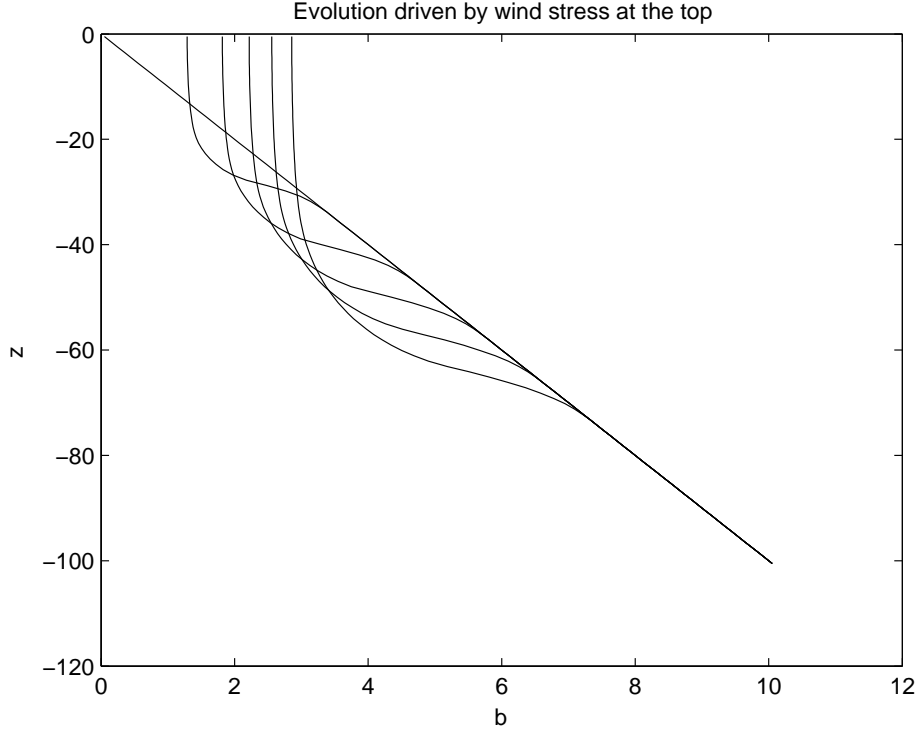


FIGURE 4.3. Buoyancy profile corresponding to the evolution of a well-mixed layer driven by wind stress, represented by a constant flux of horizontal momentum through the surface: $K_u u_z = 0.15$. As in Figure 4.2, there is a turbulent energy flux as well, given by $K_e e_z = 0.0003$. The snapshots are displayed 700 time units apart.

There are two critical values for Ri . The first one arises from considerations involving the total energy of the system, while the second follows from the details of the dynamics.

If one replaces a stably stratified, sheared flow within a thin layer $z_0 - \Delta z \leq z \leq z_0 + \Delta z$ by a homogeneous flow with the same mass and momentum, the potential energy of the layer increases, but the kinetic energy decreases. The changes in the potential and kinetic energy are, to leading order in Δz ,

$$\begin{aligned} \Delta PE &\approx \int_{-\Delta z}^{\Delta z} b(z_0)(z_0 + s) ds - \int_{-\Delta z}^{\Delta z} (b(z_0) + b_z(z_0)s)(s + z_0) ds \\ &= \int_{-\Delta z}^{\Delta z} -b_z(z_0)s^2 ds, \end{aligned}$$

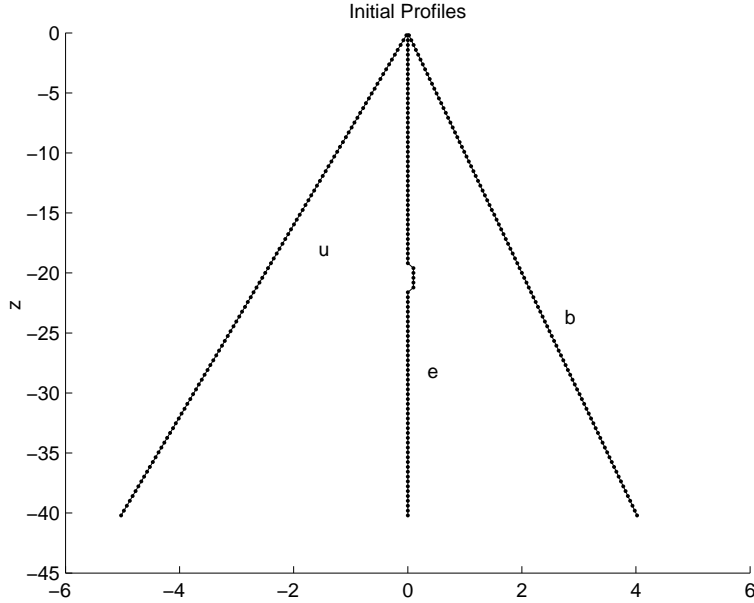


FIGURE 4.4. Qualitative initial density, velocity, and turbulent energy profile for all numerical experiments on shear instability.

$$\begin{aligned} \Delta \text{KE} &\approx \int_{-\Delta z}^{\Delta z} \frac{(u(z_0))^2}{2} ds - \int_{-\Delta z}^{\Delta z} \frac{(u(z_0) + u_z(z_0)s)^2}{2} ds \\ &= \int_{-\Delta z}^{\Delta z} \frac{(u_z(z_0))^2 s^2}{2} ds. \end{aligned}$$

Therefore, if the Richardson number is smaller than $\frac{1}{2}$, then the kinetic energy of the shear is larger than the potential energy necessary to locally uniformize the fbw; this should yield a final state where the fluid is neither stratified nor sheared, and all the extra energy has been converted into turbulence or exported to another region.

The other critical value follows from the turbulent energy equation. If $\text{Ri} < S_u/S_b$, where the S_j 's are the coefficients defining the diffusivities in (2.8), then the input of kinetic energy, $K_b b_z + K_u (u_z)^2 = l e^{1/2} (S_u - \text{Ri} S_b) u_z^2$, is positive; i.e., the potential energy sink due to mixing is smaller than the kinetic energy gain produced by the suppression of shear. This gives rise to instability.

Hence we need to consider various cases, depending on how the Richardson number of the unperturbed fbw relates to the critical value S_u/S_b and to $\frac{1}{2}$. In the discussion that follows, we will consider as initial profiles linear backgrounds of buoyancy and horizontal velocity, and a profile of turbulent energy that is zero everywhere except for a small bump included to trigger potential instabilities (see Figure 4.4). This is also the initial data for our numerical simulations.

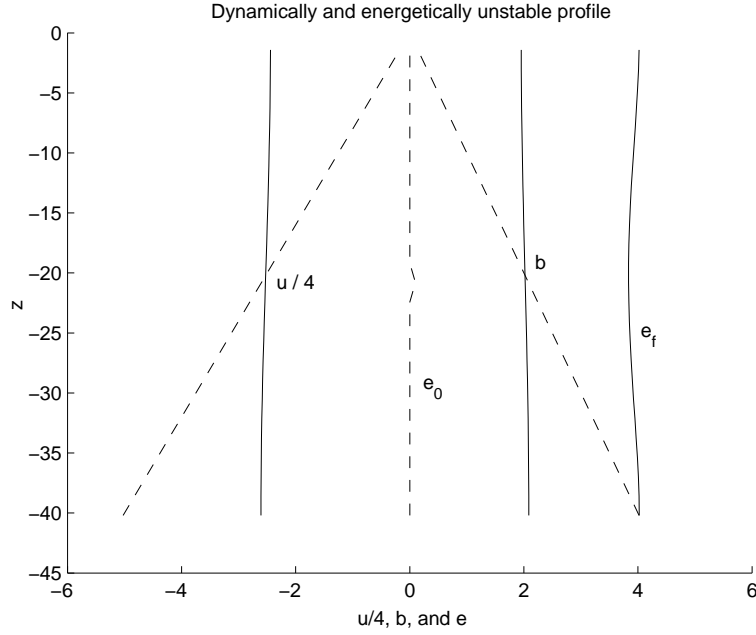


FIGURE 4.5. Evolution of a profile that is dynamically and energetically unstable. The final profile is fully homogeneous, with neither shear nor stratification, and all extra energy converted into turbulence. In this run, $S_b = S_u = S_e = 1$, and initially $B_z = -0.1$ and $U_z = 0.5$.

First, if

$$\text{Ri} < \min\left(\frac{S_u}{S_b}, \frac{1}{2}\right),$$

then any small perturbation should grow, leading to a global mixing event, able to completely overcome the stratification, and to a final state with uniform buoyancy and velocity, with all the excess energy converted into turbulence. The results of a numerical experiment confirming this scenario are plotted in Figure 4.5.

If

$$\frac{1}{2} < \text{Ri} < \frac{S_u}{S_b},$$

we expect any small initial turbulent energy to grow and to produce more mixing. On the other hand, since the total energy is not sufficient to completely mix the fluid, this process must end at some point, which can only happen if Ri grows beyond S_u/S_b . So we expect the final value of the Richardson number to be everywhere larger than the dynamical critical value. Even though the initial turbulent kinetic energy is confined to a small layer, the mixing will spread through the full depth of the fluid, and the final state will still be both stratified and sheared, but to a lesser degree than in the initial profile. This is indeed the case, as the numerical experiment displayed in Figure 4.6 shows. This scenario corresponds to the double

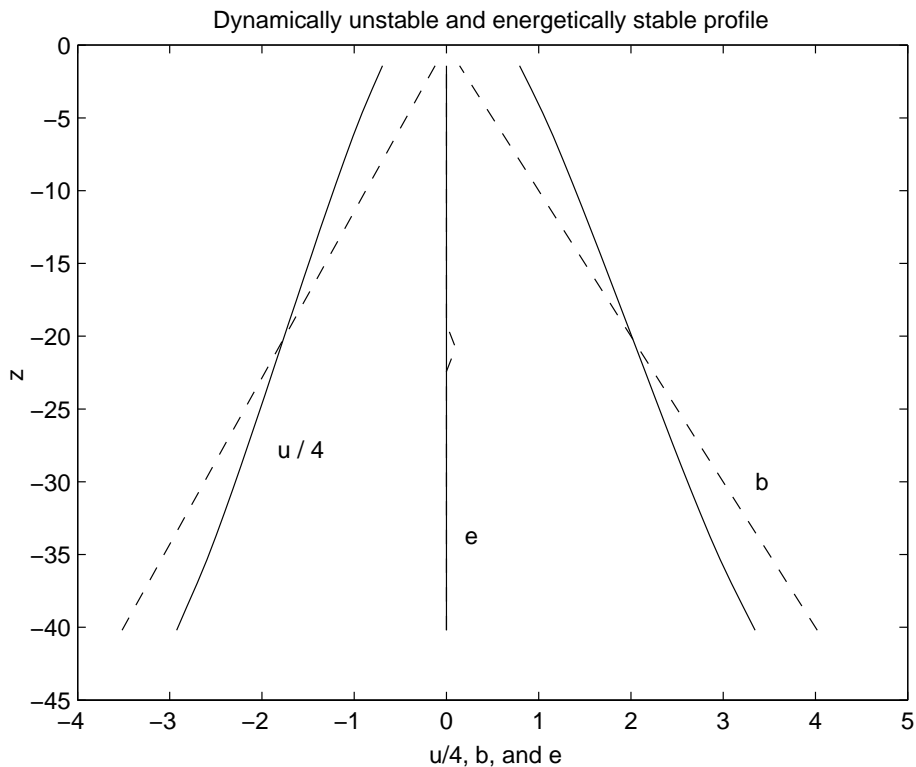


FIGURE 4.6. Evolution of a profile that is dynamically unstable yet lacks enough kinetic energy to fully mix. Part of the energy in the shear is used for mixing, but the final state has both shear and stratification. In this run, $S_b = S_u = S_e = 1$, and initially $B_z = -0.1$ and $U_z = 0.35$.

diffusive instability, where an energetically stable profile can grow unstable due to disparities in the diffusivities of the two quantities involved.

If the value of Ri is larger than the critical value S_u/S_b , then small disturbances to the main flow will have little effect. Any sufficiently small initial turbulent energy added to the flow will be consumed and transferred mainly to potential energy. If the initial turbulent energy is confined to a portion of the domain, say some layer between the depths a and b , then the mixing will take place only in a somewhat broader layer, but it will still be localized. A numerical run of this situation can be seen in Figure 4.7.

Interestingly, this situation applies even when $S_u/S_b < Ri < \frac{1}{2}$. Here the flow is stable to small perturbations, even though it has enough energy to potentially mix and become completely homogeneous. The existing turbulent energy will be transformed into potential energy faster than it can collect kinetic energy

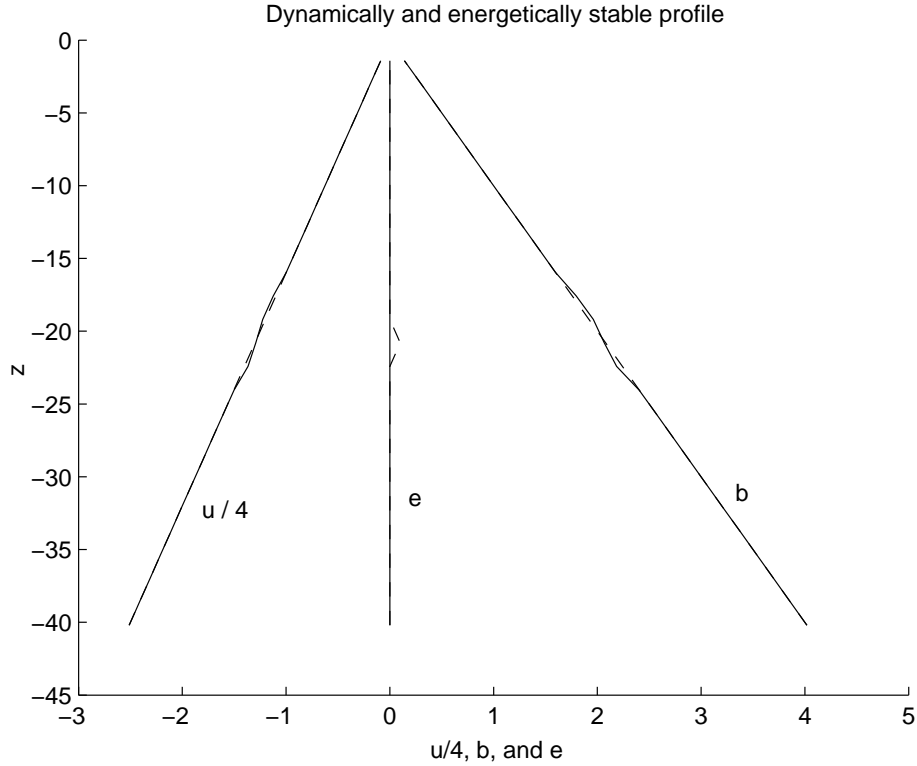


FIGURE 4.7. Evolution of a profile that is stable, both on dynamic and energetic grounds. A small patch of turbulence added to the flow yields a localized and moderate amount of mixing. In this run, $S_b = S_u = S_e = 1$, and initially $B_z = -0.1$ and $U_z = 0.25$. In this and in all remaining figures, the dashed and solid lines correspond to the initial and final profiles, respectively.

from the shear, so the turbulence will eventually disappear, not allowing any further mixing to occur. This scenario, where the state of maximal entropy is not dynamically reachable, is reminiscent of other geophysical situations, such as the high-potential-energy states in geostrophic balance with zonal winds prevailing in the atmosphere that can only acquire entropy by eliminating some potential energy through violent nonlinear instabilities, yielding mid-latitude storms.

We analyze now more general equilibrium states for the system of equations (4.1), (4.2), and (4.3). For closed systems with no-flux boundary conditions, all equilibria have $e = 0$. Yet the real ocean does have fluxes of buoyancy and horizontal momentum originating at its upper and lower boundaries, and arising from processes such as radiative heating and cooling and surface wind stress. In the presence of boundary fluxes, other relevant equilibrium states appear, with $Ri = S_u/S_b$, constant buoyancy and velocity gradients, and uniform e . We shall consider this

case first, perturbing a state with $\bar{b}_z = B'$, $\bar{u}_z = U'$, $\bar{e} = E$, and $S_b B' = -S_u (U')^2$, where B' , U' , and E are constants. Denoting the perturbation with tildes, we have

$$b = \bar{b} + \tilde{b}, \quad u = \bar{u} + \tilde{u}, \quad e = E(1 + \tilde{e}).$$

The linearization of the equations reads, with the tildes dropped,

$$(4.9) \quad \begin{aligned} b_t &= (lE^{\frac{1}{2}} S_b) \left(b_{zz} + \frac{e_z B'}{2} \right), & u_t &= (lE^{\frac{1}{2}} S_u) \left(u_{zz} + \frac{e_z U'}{2} \right), \\ e_t &= (lE^{\frac{1}{2}} S_e) e_{zz} + (lE^{-\frac{1}{2}} S_b) b_z + (lE^{-\frac{1}{2}} S_u U') 2u_z. \end{aligned}$$

Proposing solutions of the form $(b, u, e) = (b_0, u_0, e_0) e^{i(kz - \omega t)}$, system (4.9) adopts the form

$$\begin{bmatrix} \frac{i\omega}{lE^{\frac{1}{2}}} - k^2 S_b & 0 & ik \frac{S_b B'}{2} \\ 0 & \frac{i\omega}{lE^{\frac{1}{2}}} - k^2 S_u & ik \frac{S_u U'}{2} \\ \frac{ik S_b}{E} & \frac{2ik S_u U'}{E} & \frac{i\omega}{lE^{\frac{1}{2}}} - k^2 S_e \end{bmatrix} \begin{bmatrix} b_0 \\ u_0 \\ e_0 \end{bmatrix} = \begin{bmatrix} 0 \\ 0 \\ 0 \end{bmatrix}.$$

Clearly, this system has nontrivial solutions only when its determinant D is 0.

Let us set

$$x = \frac{i\omega}{lE^{\frac{1}{2}}}, \quad \alpha = k^2 S_b, \quad \beta = k^2 S_u, \quad \gamma = k^2 S_e, \quad \text{and} \quad p(x) = \frac{D}{(lE^{\frac{1}{2}})^3}.$$

Then

$$p(x) = (x - \alpha)(x - \beta)(x - \gamma) + (x - \alpha) \frac{\beta S_u (U')^2}{E} - (x - \beta) \frac{\alpha S_u (U')^2}{2E}.$$

An unstable solution where the imaginary part of ω is positive corresponds to a root of $p(x)$ where the real part of x is negative.

We will show below that a necessary and sufficient condition for stability is that

$$(4.10) \quad \text{Ri} \left(\text{Ri} + \frac{S_e}{S_b} \right) \geq \frac{1}{2} \left(1 + \frac{S_e}{S_b} \right),$$

where $\text{Ri} = S_u/S_b$ is the Richardson number for the unperturbed profile. It follows easily that, if the Richardson number is smaller than $\frac{1}{2}$, then the equilibrium is unstable, and if it is bigger than $\sqrt{2}/2$, it is stable, independently of the value of S_e . For values of Ri in between $\frac{1}{2}$ and $\sqrt{2}/2$, the stability depends on S_e/S_b through condition (4.10). This potential instability of fbws with $\text{Ri} > \frac{1}{2}$ agrees with similar results in other models [1, 4], as well as with empirical [10] and laboratory [16] evidence. The question of the long-term behavior of the system in the unstable regime will be explored in subsequent work.

To prove condition (4.10), notice that the sum of the real part of the three roots of $p(x)$ is $\alpha + \beta + \gamma$. If there is a root x_1 with real part larger than this number, then there must exist another root with negative real part, yielding instability. Moreover, if there are no negative real roots of $p(x)$, then if there are roots with negative

real part, they must come in complex conjugate pairs, and the third root must be positive and real. Then the existence of a *real* root larger than $\alpha + \beta + \gamma$, a sufficient condition for instability, also becomes necessary.

Now,

$$p(\alpha + \beta + \gamma) = (\beta + \gamma)(\alpha + \gamma)(\alpha + \beta) + \left((\beta + \gamma)\beta - (\alpha + \gamma)\frac{\alpha}{2} \right) \frac{S_u(u')^2}{E},$$

so that, if

$$(4.11) \quad (\beta + \gamma)\beta \geq (\alpha + \gamma)\frac{\alpha}{2},$$

there can be no real root larger than $\alpha + \beta + \gamma$, since $p(\alpha + \beta + \gamma) > 0$ and $p'(x) > 0$ for all $x > \alpha + \beta + \gamma$. Since (4.11) implies that $\beta > \frac{\alpha}{2}$, we see that $p'(x) > 0$ for all $x < 0$, and, since

$$p(0) = (lE^{\frac{1}{2}})^3 \left(-\alpha\beta\gamma - \alpha\beta \frac{S_u U^2}{2E} \right) < 0,$$

there are no negative real roots, and so the system is stable. On the other hand, if (4.11) is not satisfied, then for small enough E (or for small enough k), $p(\alpha + \beta + \gamma) < 0$, and since $\lim_{x \rightarrow \infty} p = +\infty$, there is a positive real root larger than $\alpha + \beta + \gamma$, so the system is unstable.

Finally, notice that (4.11) is equivalent to

$$(S_u + S_e)S_u \geq (S_b + S_e)\frac{S_b}{2},$$

which yields condition (4.10).

When $e = 0$, steady solutions to (4.1), (4.2), and (4.3) exist for any $\bar{b}(z)$ and $\bar{u}(z)$. Perturbing these equilibria yields, to leading order,

$$(4.12) \quad b_t = (le^{\frac{1}{2}} S_b \bar{b}_z)_z, \quad u_t = (le^{\frac{1}{2}} S_u \bar{u}_z)_z, \quad e_t = le^{\frac{1}{2}} (S_b \bar{b}_z + S_u (\bar{u}_z)^2).$$

Notice that the right-hand side of the system is independent of b and u . If the Richardson number of the equilibrium state $\text{Ri} = -\bar{b}_z/(\bar{u}_z)^2$ is everywhere larger than the critical dynamical value S_u/S_b , and b_z is bounded away from 0, then there is a positive constant C such that $e_t < -Ce^{1/2}$ everywhere in the domain. This implies that $e_t(z, t) \leq (e(z, 0)^2 - (C/2)t)^2$, so the solutions to system (4.12) will reach $e = 0$ in a time smaller than $\max_{-H \leq z \leq 0} 2(e(z, 0))^2/C$. Hence the equilibrium is stable. On the other hand, if the Richardson number is smaller than S_u/S_b at some point in the domain, e will grow at this depth until higher-order terms take over, so the equilibrium is unstable.

5 Two-Dimensional Applications

In this section we explore some two-dimensional applications of our model. This enables us to consider interesting scenarios where the dynamics of incompressible fluid motion can interact, in a variety of ways, with the turbulent diffusion processes. In particular, two-dimensional fluids can sustain waves, which carry energy, both potential and kinetic. Turbulent mixing, on the other hand, can serve as a drain for this energy, thus damping the waves. Here we explore numerically some of these possible interactions.

In two dimensions (x, z) , and without ambient rotation, the equations in (2.1), (2.2), and (2.7) assume the form

$$(5.1) \quad b_t + \nabla \cdot (b\vec{u}) = \nabla \cdot (K_b \nabla b),$$

$$(5.2) \quad u_t + \nabla \cdot (u\vec{u}) + P_x = \nabla \cdot (K_u \nabla u),$$

$$(5.3) \quad \left(zb + \frac{|u|^2}{2} + e \right)_t + \nabla \cdot \left(\left(zb + \frac{|u|^2}{2} + e + P \right) \vec{u} \right) \\ = \nabla \cdot \left(K_e \nabla e + K_b z \nabla b + K_u \nabla \frac{|u|^2}{2} \right),$$

where now $\vec{u} = (u, w)$ and $\nabla = (\partial_x, \partial_z)$.

5.1 Breaking Waves

In this subsection the two-dimensional model above is used to study the effect that breaking waves exert on mixing. It is a well-known fact that, in order to conserve momentum, shocks need to dissipate kinetic energy. Since our model preserves the total energy, the energy dissipated needs to be converted into turbulence, and then into potential energy through mixing.

In order to isolate breaking waves as cleanly as possible, we shall initialize our numerical experiments with small-amplitude waves, chosen as right-propagating modes of the linearized equations. The main expected effect of the weak nonlinearity is that it will slowly modulate the shape of the wave until it breaks. From then on, the combined effects of wave overturning and sharp velocity gradients will generate turbulent energy, locally mixing the flow. Hence we shall consider small perturbations of an equilibrium state consisting of a background stratification profile at rest, homogeneous in the horizontal direction. The domain of integration is periodic in x and has rigid boundaries at heights $z = z_0$ and $z = z_1$, with no-flux conditions $w(x, t, z_0) = w(x, t, z_1) = 0$.

Decomposing the buoyancy and pressure into a background state and a perturbation,

$$b(x, z) = \bar{b}(z) + b'(x, z), \quad P(x, z) = \bar{P}(z) + P'(x, z),$$

where $\bar{P}_z + \bar{b} = 0$, the linearization of the equations in (5.1), (5.2), and (5.3) reads

$$(5.4) \quad \begin{aligned} b_t + \bar{b}_z w &= 0, & u_t + P_x &= 0, \\ u_x + w_z &= 0, & P_z + b &= 0, \end{aligned}$$

where we have dropped the primes to simplify notation. Simple algebraic manipulations yield

$$(5.5) \quad w_{zzt} - \bar{b}_z w_{xx} = 0,$$

showing the hyperbolic behavior of the system (5.4) when the stratification is stable ($\bar{b}_z < 0$) and suggesting wavelike solutions in the horizontal direction. Indeed, if $(f(z), \mu)$ solves the eigenvalue problem

$$(5.6) \quad f'' = \mu \bar{b}_z f,$$

$$(5.7) \quad f(z_0) = f(z_1) = 0,$$

then system (5.4) has traveling-wave solutions given by

$$(5.8) \quad \begin{aligned} u(x, z, t) &= -\sigma(x - ct) f'(z), \\ b(x, z, t) &= -\frac{1}{c} \bar{b}_z(z) \sigma(x - ct) f(z), \\ w(x, z, t) &= \sigma'(x - ct) f(z), \\ P(x, z, t) &= cu(x, z, t), \end{aligned}$$

where $c = 1/\sqrt{\mu}$. If one such wave is given as initial data to the fully nonlinear system (2.4), (2.5), (5.1), (5.2), and (5.3), it is to be expected that nonlinearity will cause the wave to deform and break, thus producing mixing. We have studied this situation for two different background stratifications, corresponding to a continuously stratified profile and to a two-layer fbw, respectively.

To solve the equations, we use finite differences in conservation form. The dependent variables are the average values of b , u , and E over spatial cells. They are updated by computing their associated fluxes—advective, dynamic, and diffusive—at the cell's interfaces, through simple interpolation and finite differencing. For time stepping, we have adopted a second-order predictor-corrector scheme.

The calculation of the pressure P is more subtle, since it follows from enforcing the global incompressibility constraint. We begin the numerical runs with a velocity field that satisfies the no-flux condition at the top and bottom boundaries. This implies that

$$\int_{z_1}^{z_0} u_x(x, z, 0) dz = 0.$$

In order to preserve the no-flux condition at later times, we need that

$$(5.9) \quad 0 = \int_{z_1}^{z_0} u_{xt}(x, z, t) dz = \int_{z_1}^{z_0} (K_u u_x)_x - (u^2)_{xx} - P_{xx} dz.$$

To enforce this condition, we decompose the pressure $P = P_0(x, z, t) + P_1(x, t)$ into two parts, one purely hydrostatic, $P_0(x, z, t) = \int_{z_1}^z -b(x, s, t)ds$, and P_1 depth independent, representing the effects of the rigid boundaries. P_1 is obtained at each time t by solving the problem

$$(z_0 - z_1)(P_1)_{xx} = \int_{z_1}^{z_0} (K_u u_x)_x - (u^2)_{xx} - (P_0)_{xx} dz,$$

$$P_1(0, t) = P_1(L, t) = 0,$$

so that equation (5.9) is satisfied and the pressure field is horizontally periodic. The integrals are computed numerically using the trapezoidal rule.

Finally, the vertical velocity w is obtained diagnostically from the vertical integration of the horizontal divergence u_x .

Continuous Stratification

For the continuously stratified profile, we have chosen, for analytical simplicity, $\bar{b} = \frac{1}{z}$, with $-21 \leq z \leq -1$. With this choice, the eigenvalue problem (5.6) has simple solutions; we have adopted the first baroclinic mode

$$f = \sqrt{|z|} \sin\left(2\pi \frac{\log(|z|)}{\log(21)}\right)$$

corresponding to

$$c = \sqrt{\frac{\pi}{\log(21)} + \frac{1}{4}}.$$

The choice for an initial horizontal profile $\sigma(x)$ is arbitrary; we have adopted a sinusoidal wave:

$$\sigma(x) = 0.7 \sin\left(2\pi \frac{x}{L}\right)$$

where $L = 80$ is the horizontal extent of the domain.

In Figure 5.1 we display a closeup of $-6 \leq z \leq -1$ for various times, both before and after the wave breaking, which takes place around $t = 20$. Notice the larger spacing between isoclines in the region downstream of the shock, indicating that an attenuation of the buoyancy gradients has occurred due to mixing.

Additional evidence of mixing is displayed in Figure 5.2, showing the time evolution of the mixing measure S and its mean variation between the times of the recorded values. One clearly sees the increase in the rate of mixing beginning precisely at the time of the breaking of the wave and continuing while the intensity of the shock increases.

Two-Layer Flow

To represent a two-layer flow, the background stratification should consist of a step function, with $\bar{b} = 0$ for $z_1 \leq z < \bar{z}$, and $\bar{b} = k$ for $\bar{z} \leq z \leq z_0$, where $\bar{z} - z_0$ is the height of the bottom layer and $z_0 - \bar{z}$ is the height of top layer. The problem with taking this approach is that linear perturbations to such a discontinuous profile

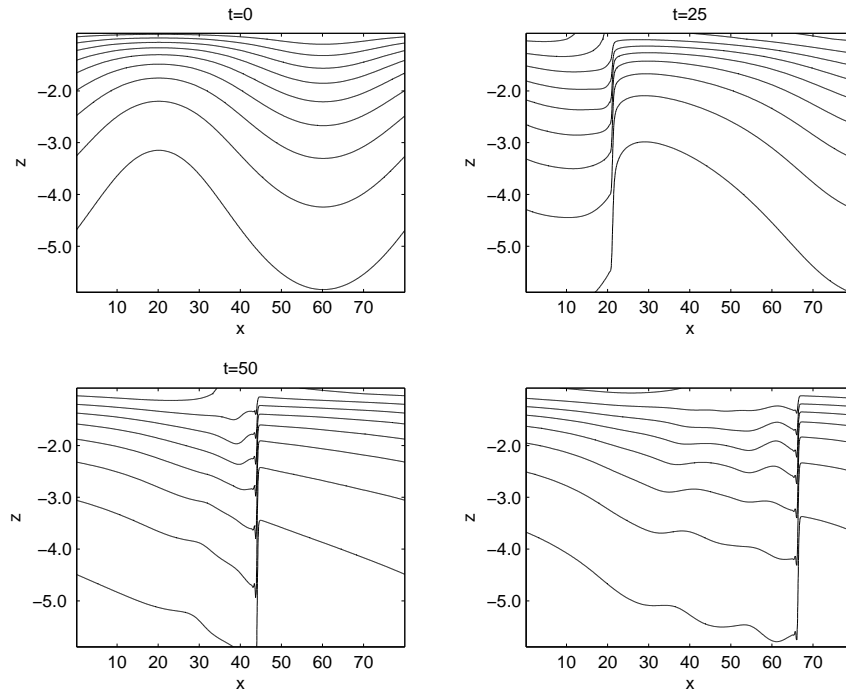


FIGURE 5.1. Detail of the evolution of a breaking internal wave on a continuously stratified profile.

involve δ -functions, which are difficult to handle numerically. The simplest way around this problem is to use instead a smooth mollification of a step function as a background profile.

For concreteness, consider a domain periodic in x , with period $L = 100$, and vertically bounded between $z_0 = 0$ and $z_1 = -50$. We would like the background to consist of two layers: a bottom layer of height 10 and an upper one of height 40. With this background stratification, the solution f_0 to the eigenvalue problem (5.6) is piecewise linear, with a discontinuity in the derivative at $z = -40$. If we mollify the background arbitrarily, finding a solution to (5.6) in closed form may be out of the question. Instead of resorting to solving this eigenvalue problem numerically, we may invert the question, choosing a mollification of the *solution* f_0 , and then *computing* the corresponding mollified background profile. To this end, we pick arbitrarily $c = 1$ and a smooth function f that is close to f_0 . The advantage of taking this path is that from there it is straightforward to determine \bar{b} : we only need to integrate the simple ODE

$$\bar{b}' = \frac{f}{f''}.$$

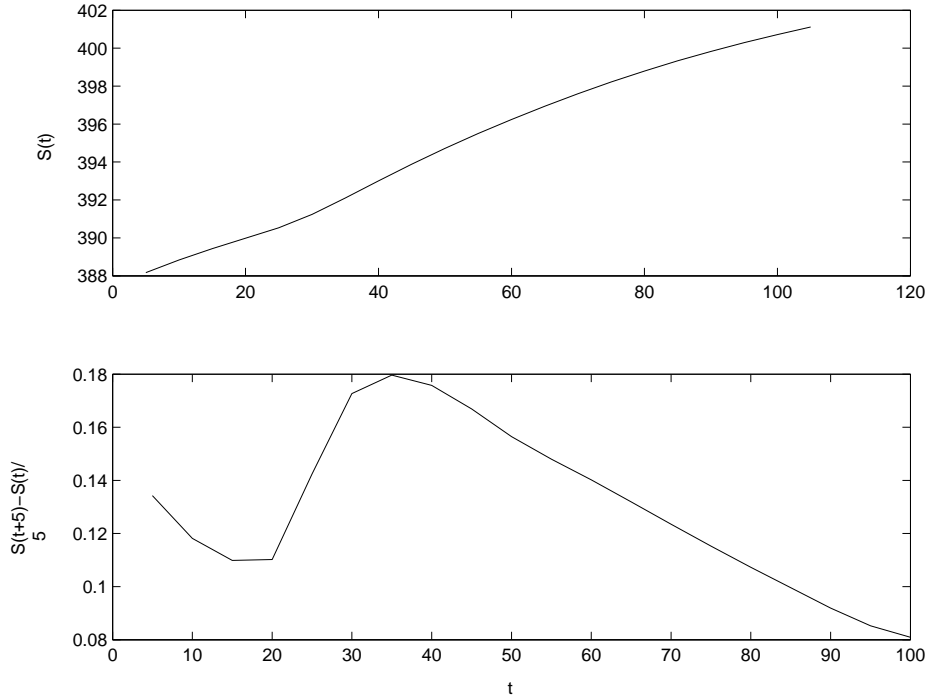


FIGURE 5.2. Time evolution of the mixing measure S for a breaking internal wave on a continuously stratified profile.

For our numerical experiment, we have adopted

$$(5.10) \quad f(z) = \int_{-50}^z \Phi\left(\frac{s+40}{2}\right) ds - \left(1 + \frac{z}{50}\right) \int_{-50}^0 \Phi(s+40) ds$$

where Φ is the error function given by

$$\Phi(x) = \int_{-\infty}^x \frac{e^{-s^2/2}}{\sqrt{2\pi}} ds.$$

The initial horizontal profile is again sinusoidal,

$$\sigma(x) = \frac{3}{40} \sin\left(2\pi \frac{x}{L}\right).$$

Figure 5.3 shows the background stratification \bar{b} .

The numerics again show enhanced mixing after the shock formation, which takes place around $t = 135$. Figure 5.4, a closeup of the interface between the two layers, displays the evolution of two isopycnals lying in the mollified transition between the top and bottom layer. The steepening and breaking of the wave is

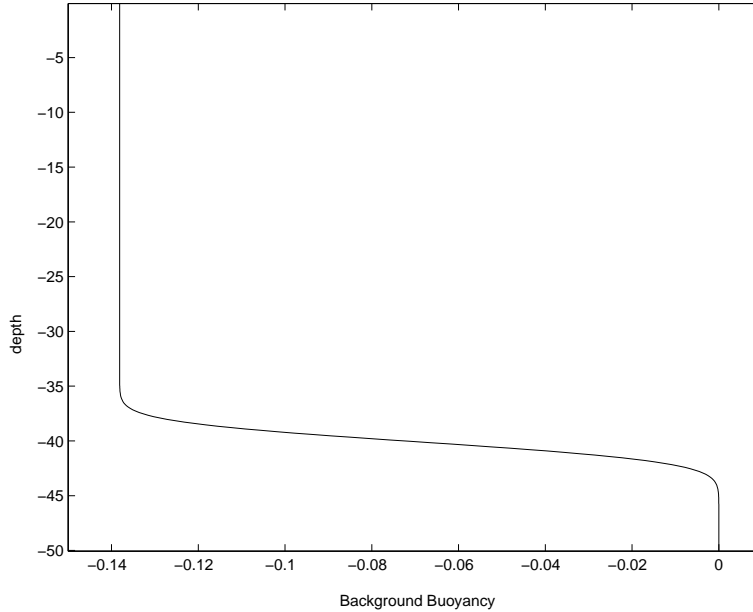


FIGURE 5.3. Mollified two-layer profile.

clearly visible. Figure 5.5, on the other hand, shows the time evolution of the mixing measure S and its rate of change. The initial profile for the normalized density, $\bar{b} + b$, has, at time zero, regions where the stratification is mildly unstable, that is, $\bar{b}_z + b_z > 0$. Due to this, some turbulent energy develops from the beginning of the run, explaining the small positive derivative of S from the start of the numerical experiment. Nonetheless, there is still a remarkable increase in the rate of mixing when the wave breaks.

6 Conclusions

In this article we have shown the versatility of turbulent diffusive models as conceptual tools for the study of fluid mixing in geophysical contexts. The simplest of these models solve standard fluid equations in the large scales and replace the dynamics of the unresolved scales by nonlinear diffusion, with a diffusivity proportional to the local turbulent energy content. The existence of unresolved scales is not just a matter of computational grid size: the equations used for the large scales are based on physical hypotheses, such as the hydrostatic balance, that generally do not hold in the small, turbulent scales. Hence turbulent diffusive modeling is useful not only as a numerical strategy but also as an attractive mathematical reduction of the full Navier-Stokes equations.

We have applied the model to describe the appearance and dynamical evolution of sharply defined, well-mixed layers and to contrast the properties of layers stirred

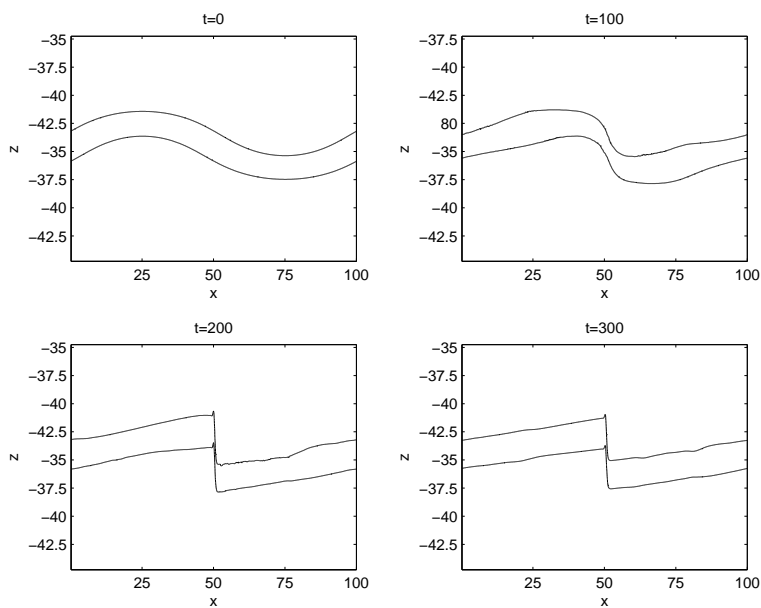


FIGURE 5.4. Closeup of the evolution of a breaking internal wave on a mollified two-layer background profile.

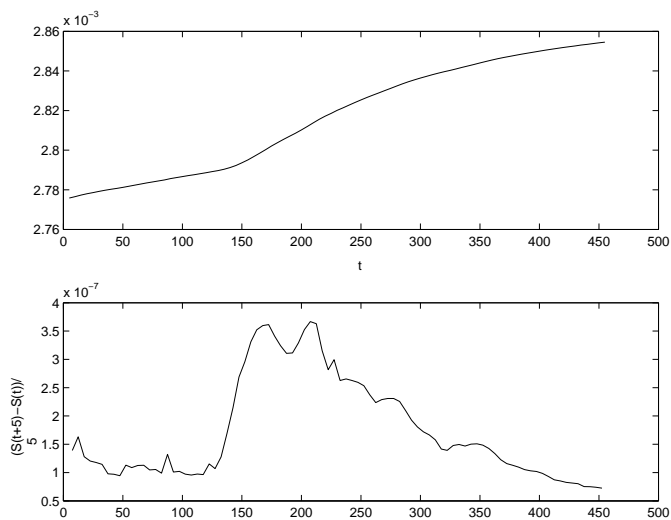


FIGURE 5.5. Evolution of the mixing measure for a breaking internal wave on a mollified two-layer background profile. The top figures show the mixing measure S itself, while the lower one shows its rate of change, with a sharp increase when the wave breaks.

by buoyancy and turbulence fluxes at the ocean's surface with those which extract their energy from shear instability at their base. We have also used the model to discuss the shear instability of stratified flows and noted the important distinction between global constraints, such as the availability of enough energy for mixing, from local constraints related to the fluid's detailed dynamics. Another application that we have touched upon is fluid mixing by internal breaking waves, both in two-layer flows and under continuous stratification.

Finally, we have introduced a novel measure of mixing, based on considerations analogous to those at the core of statistical mechanics. Turbulent diffusive simulations of two fluid layers stirred at their interface show a tendency of the flow to achieve a final state of maximal mixing, consistent with just the coarsest dynamical constraints (i.e., global conservation of mass and energy). This mixing measure is also a useful tool to monitor flows. In particular, its growth rate shows a pronounced increase when internal waves break.

Acknowledgments. We would like to thank an anonymous referee for a very careful, detailed report, which has helped us improve this paper significantly. The work of Fabio A. Tal was supported by grant #200800/09-1 from Conselho Nacional de Desenvolvimento Científico e Tecnológico (CNPq), Brasil.

Bibliography

- [1] Abarbanel, H. D. I.; Holm, D. D.; Marsden, J. E.; Ratiu, T. Richardson number criterion for the nonlinear stability of three-dimensional stratified flow. *Phys. Rev. Lett.* **52** (1984), no. 26, 2352–2355.
- [2] Balmforth, N. J.; Llewellyn Smith, S. G.; Young, W. R. Dynamics of interfaces and layers in a stratified turbulent fluid. *J. Fluid Mech.* **355** (1998), 329–358.
- [3] Boucher, C.; Ellis, R.; Turkington, B. Derivation of maximum entropy principles in two-dimensional turbulence via large deviations. *J. Statist. Phys.* **98** (2000), no. 5-6, 1235–1278.
- [4] Canuto, V. M.; Howard, A.; Cheng, Y.; Dubovikov, M. S. Ocean turbulence. I. One-point closure model—momentum and heat vertical diffusivities. *J. Phys. Oceanogr.* **31** (2001), no. 6, 1413–1426.
- [5] Howard, L. N. Note on a paper of John W. Miles. *J. Fluid Mech.* **10** (1961), 509–512.
- [6] Jacobson, T.; Milewski, P. A.; Tabak, E. G. A closure for mixing at internal breaking waves. In preparation, 2003.
- [7] Landau, L. D.; Lifshitz, E. M. *Statistical physics*. Pergamon, Oxford, England, 1980.
- [8] Lorenz, E. N. Available potential energy and the maintenance of the general circulation. *Tellus* **7** (1955), 157–167.
- [9] Majda, A. J.; Kramer, P. R. Simplified models for turbulent diffusion: theory, numerical modelling, and physical phenomena. *Phys. Rep.* **314** (1999), no. 4-5, 237–574.
- [10] Martin, P. J. Simulation of the mixed layer at OWS November and Papa with several models. *J. Geophys. Res.* **90** (1985), 903–916.
- [11] Mellor, G. L.; Yamada, T. A hierarchy of turbulent closure models for planetary boundary layers. *J. Atmos. Sci.* **31** (1974), 1791–1806.
- [12] Miles, J. W. On the stability of heterogeneous shear flows. *J. Fluid Mech.* **10** (1961), 496–508.
- [13] Peltier, W. R.; Caulfield, C. P. Mixing efficiency in stratified shear flows. *Annual review of fluid mechanics*, Vol. 35, 135–167. Annual Reviews, Palo Alto, Calif., 2003.

- [14] Strang, E. J.; Fernando, H. J. S. Entrainment and mixing in stratified shear flows. *J. Fluid Mech.* **428** (2001), 349–386.
- [15] Tabak, E. G.; Tal, F. A. Turbulent mixing of stratified flows. *Cubo Mat. Educ.* **6** (2004), in press.
- [16] Webster, C. A. G. An experimental study of turbulence in a density stratified shear flow. *J. Fluid Mech.* **19** (1964), 221–245.

ESTEBAN G. TABAK
Courant Institute
251 Mercer Street
New York, NY 10012-1185
E-mail: tabak@cims.nyu.edu

FABIO A. TAL
Courant Institute
251 Mercer Street
New York, NY 10012-1185
E-mail: tal@cims.nyu.edu

Received March 2003.